S & M 4167

# Large-scale Geographic Information System-based Vulnerability Assessment of Black-ice-related Expressway Accidents Using Entropy Weighting

Seok Bum Hong,<sup>1,2</sup> Moon-soo Song,<sup>3</sup> and Jaejoon Lee<sup>4\*</sup>

<sup>1</sup>Interdisciplinary Program for Crisis, Sungkyunkwan University, 2066, Seobu-ro, Jangan-gu, Suwon-si 16419, Republic of Korea <sup>2</sup>Advanced Railroad Civil Engineering Division, Korea Railroad Research Institute, 176, Cheoldobangmulgwan-ro, Uiwang-si 16105, Republic of Korea <sup>3</sup>Smart Infra Research Institute, Gangneung-Wonju National University, 7, Jukheon-gil, Gangneung-si 25457, Republic of Korea <sup>4</sup>Department of Fire Safety Engineering, Jeonju University, 303, Cheonjam-ro, Wansan-gu, Jeonju-si 55069, Republic of Korea

(Received May 8, 2025; accepted September 4, 2025)

Keywords: black ice, GIS analysis, entropy weighting, expressway safety, climate risk

Black ice is difficult to detect with the naked eye because it reflects the color of the road surface. It often forms rapidly owing to freezing rain and leads to severe traffic accidents, particularly on expressways. To reduce the risk of casualties, it is essential to assess the vulnerability of expressway sections to black-ice-related accidents. In his study, we present a large-scale assessment of such vulnerability, aimed at providing a quantitative foundation for preventive measures and rational resource allocation. Ten contributing factors were selected using the Intergovernmental Panel on Climate Change (IPCC) Climate Change Vulnerability Assessment Framework and categorized into three groups: exposure, sensitivity, and adaptive capacity. Each factor was normalized and analyzed using entropy weighting within a geographic information system (GIS) environment. The exposure factors included hillshade (mean: 94.76), precipitation (mean: 219.78 mm), humidity (mean: 70.97%), and temperature (mean: 2.01 °C). Sensitivity factors comprised slope (mean: 7.5°), curvature (mean: 0.15), traffic volume (mean: 62073 vehicles), bridge length (mean: 1452.06 m), and tunnel count (mean: 2.33). Adaptive capacity was represented by the density of 119 Emergency Rescue Centers (mean: 0.01). The final vulnerability index had an average of 0.96 with a standard deviation of 0.20. These results provide a practical basis for formulating black ice accident prevention strategies and optimizing the allocation of safety-related resources. The findings also offer valuable policy insights for winter road safety planning and infrastructure vulnerability management.

#### 1. Introduction

Black ice commonly forms in dark and cold areas, such as roads shaded by frost, freezing rain, or melting snow. It creates a thin, transparent layer on asphalt that is nearly indistinguishable from the normal road surface, earning it the name "black ice". (1) This phenomenon often results in severe traffic accidents, particularly when it forms rapidly owing to freezing rain. Freezing rain refers to supercooled precipitation that remains liquid at or below 0 °C and freezes immediately upon contact with subzero road surfaces, rendering its location and intensity difficult to predict. (2) From 2015 to 2019, fatalities from black-ice-related accidents in South Korea were four times higher than those from snowy road conditions, indicating a significantly greater risk. (3) South Korea, the study area, experiences four distinct seasons, with winter temperatures frequently falling below -10 °C. Its geography—surrounded by oceans on three sides and containing numerous inland water bodies such as rivers and lakes—contributes to a high potential for black ice formation. (4) Examples of black ice accidents include a multi-vehicle collision on the Sangju-Yeongcheon Expressway on December 14, 2019, which resulted in seven fatalities and 32 injuries, (5) and another involving 41 vehicles on National Route 33 in Gyeongsangnam-do on January 6, 2020, which left 10 individuals injured. (6) These unexpected, high-casualty events underscore the need for proactive vulnerability assessments by expressway section. Vulnerability to black ice varies spatially depending on factors such as terrain, climate, and traffic volume. Accordingly, expressway management organizations, such as the Korea Expressway Corporation, must rationally allocate countermeasure budgets based on regional characteristics. In this study, we highlight the importance of conducting large-scale vulnerability assessments across expressway sections, incorporating regional meteorological and spatial differences to support the development of effective countermeasures and targeted investments. In this context, "large-scale" refers to spatial analysis at the national or quasi-national level—for instance, Korea's nationwide expressway network or a state-level scope in federal countries such as the United States. The results of this study are expected to contribute to evidence-based policy decisions for winter road safety, particularly by supporting the strategic allocation of resources to regions with elevated black ice vulnerability.

Previous studies have attempted to estimate the vulnerability of roadways to black ice in advance. Many of these studies visualized black-ice-related indicators, such as road surface temperature, using geographic information system (GIS) tools; however, their analyses were limited to localized areas. For instance, some studies modeled black ice occurrence within GIS environments, (7,8) but these focused solely on forecasting black ice formation without evaluating the associated traffic accident vulnerability. Other studies aimed to predict general traffic accidents by integrating various contributing factors but did not specifically address black ice, assign relative weights to variables, or incorporate GIS-based spatial analysis. (9-11) Additionally, several investigations employed pavement-embedded sensors to monitor surface temperature and identify potentially hazardous sections. (12-14) Although road temperature is a critical factor in black ice formation, these sensor-based approaches often excluded essential contextual variables such as terrain, climate, and traffic volume, and remained limited in spatial coverage.

Further studies have examined the characteristics of winter road weather and temperature variation, (15,16) and some incorporated GIS-based analyses of temperature change. However, the limited number of variables and the narrow geographic scope rendered these studies insufficient for comprehensive black ice accident estimation. Since road weather conditions typically extend across broad areas, distinguishing location-specific risk in regional-scale studies remains challenging. Other researchers developed predictive models for road surface temperature using terrain, roadway design, traffic volume, and meteorological data. (17–19) While these studies identified relevant factors and implemented prediction techniques, they did not assess black ice vulnerability by road segment, primarily owing to the lack of GIS integration. Nevertheless, the terrain, climate, and traffic variables utilized in those studies were found to be relevant and were therefore incorporated into the present research.

Various technologies have been proposed as countermeasures for black ice and other roadway hazards, including safety indicator lights, (14,20) AI-based early warning systems, (21,22) intelligent snow and ice removal technologies, (13,23) and surface ice detection sensors. (13,24) However, the effective implementation of these technologies requires the prior identification of key contributing factors for black ice accident risk, along with a large-scale, GIS-based vulnerability assessment of expressways. Previous studies either concentrated primarily on road surface temperature despite utilizing GIS or considered topographic, climatic, and traffic-related variables without integrating GIS methods. Moreover, most assessments were limited to regional scopes. Therefore, a comprehensive, large-scale vulnerability assessment that incorporates weighted black ice risk factors is essential to support the efficient deployment of countermeasures.

In this study, we identify the key factors contributing to black-ice-related traffic accidents on large-scale expressways and analyze their spatial vulnerability using a GIS-based approach. The study area includes the entire national expressway network of South Korea. The analysis incorporates ten variables associated with black ice incidents, all derived through GIS-based methods: hillshade, total winter precipitation (rain and snow), average winter humidity, average winter temperature, slope, curvature, section-level traffic volume, total bridge length (m), the total number of tunnels, and the density of 119 Emergency Rescue Centers.

Each factor was categorized as either exposure, sensitivity, or adaptive capacity based on the Intergovernmental Panel on Climate Change (IPCC) Climate Change Vulnerability Assessment Framework. (25) Hillshade was calculated from a digital elevation model (DEM) with a 5 m resolution and averaged over the time period from 08:00 to 13:00. All selected variables were normalized and converted into GIS layers. These layers were subsequently overlaid using entropy-based weighting to assess the spatial vulnerability of each expressway section at a large scale.

#### 2. Methodology

In this study, we used a GIS-based approach to assess the vulnerability of expressway sections to black-ice-related traffic accidents by spatially overlaying ten factors classified according to the IPCC Climate Change Vulnerability Assessment Framework: exposure, sensitivity, and adaptive capacity. Figure 1 shows the flowchart of the overall assessment

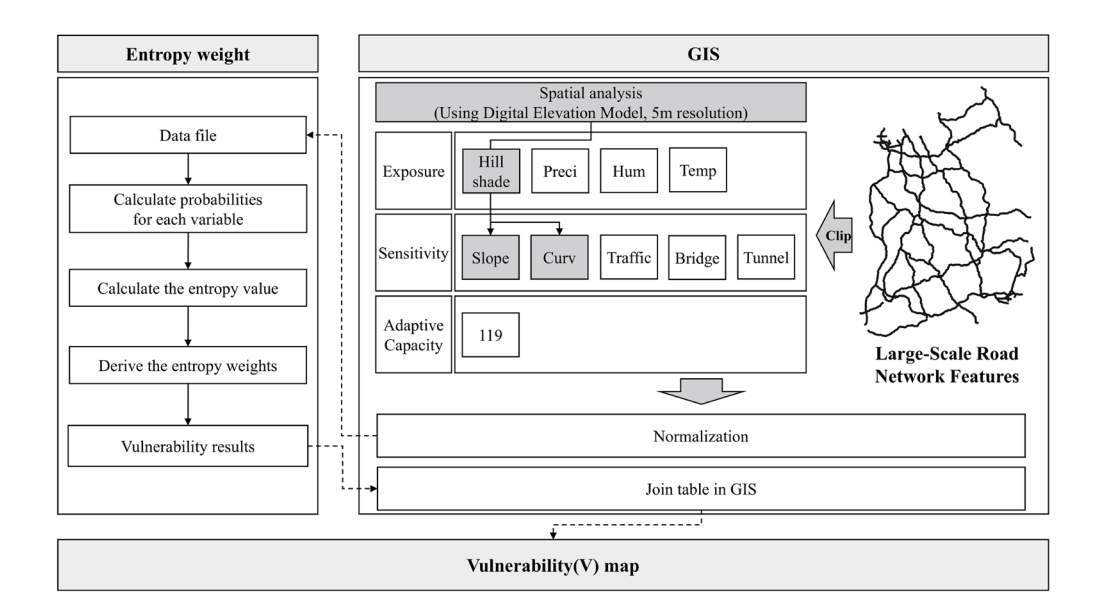


Fig. 1. Flowchart of black ice traffic accident vulnerability assessment process.

process. The exposure category includes hillshade, precipitation, humidity, and temperature, the sensitivity category comprises slope, curvature, traffic volume, bridge length, and tunnel count, and the adaptive capacity category consists of the density of 119 Emergency Rescue Centers, which serve as Korea's national emergency response facilities.

The factor maps were clipped to the expressway feature dataset in GIS, and the corresponding values were normalized. Entropy weighting was applied to each factor through the following three steps: (1) calculating the probability distribution of each variable, (2) computing the entropy values, and (3) deriving the final entropy weights. The resulting black ice vulnerability index was visualized within the GIS environment and presented as a spatial vulnerability map.

#### 2.1 Vulnerability framework and factor definitions

Table 1 shows the definitions and characteristics of each factor selected on the basis of the IPCC vulnerability assessment framework and the GIS-based analysis conducted in this study. Each variable was selected not only for its availability and spatial coverage, but also for its direct relevance to black ice formation and accident vulnerability. Meteorological factors such as low temperature, high humidity, and high precipitation are known to increase the likelihood of surface icing. Topographic variables such as slope and curvature affect vehicle control on icy roads, while traffic volume increases exposure to potential accidents. Infrastructure elements, including bridge length and tunnel count, are highly susceptible to freezing due to air exposure or shading. Finally, the density of emergency rescue centers reflects the capacity to respond effectively in areas of high vulnerability.

The analysis focused solely on national expressways in South Korea, with a total of 30 expressways included in the study. Expressways were selected as the subject of analysis owing to

estimation

Variable range GIS analysis method Category Factor Symbol Unit Hillshade Η 0 - 255Spatial analysis P **IDW** Precipitation >0 mm Exposure Humidity Hu 0 - 100% **IDW** Temperature Т °C IDW -15 to10 S Spatial analysis Slope 0 - 90Degrees Curvature C -4 to 4 Spatial analysis Sensitivity Traffic volume Tr >0 Count Attribute data В Attribute data Bridge length >0 m Tunnel count Attribute data Tu >0 Count 119 Emergency Rescue Kernel density O >0 Adaptive capacity

Table 1
Factors used for black ice traffic accident vulnerability analysis based on the IPCC framework and GIS methodologies.

Center density

their high travel speeds and the correspondingly elevated severity of traffic accidents that occur under black ice conditions. This scope enables a focused evaluation of infrastructure segments that exhibit high vulnerability to black-ice-related traffic accidents.

Hillshade is a dimensionless value, with higher values indicating greater surface illumination. As it is inversely correlated with black ice vulnerability, its reciprocal was used for calculating the vulnerability index. Precipitation represents the total accumulation over a defined winter period (mm), while humidity and temperature represent averages during the same period, expressed in percent (%) and degrees Celsius (°C), respectively. Slope ranges from 0 to 90 degrees, and curvature is a dimensionless value ranging from –4 to 4; larger absolute values indicate sharper changes in road geometry.

Traffic represents the number of vehicles passing through each expressway section over a defined time period. Bridge length denotes the total length of bridges within each section (m). Owing to exposure on both the upper and lower surfaces, bridges are more susceptible to black ice formation as a result of increased heat loss. Tunnel count indicates the total number of tunnels per expressway section. Tunnel entrances and exits are frequently shaded, resulting in lower surface temperatures and an elevated risk of black ice formation. Finally, the density of 119 Emergency Rescue Centers—South Korea's national emergency response facilities—was calculated using kernel density analysis and is represented as a dimensionless value greater than zero.

The variables hillshade, slope, and curvature were derived through the spatial analysis of a DEM. Precipitation, humidity, and temperature were interpolated by the inverse distance weighting (IDW) method, based on meteorological data from disaster prevention weather stations. The density of 119 Emergency Rescue Centers was calculated using kernel density estimation applied to point-based data. All spatial datasets generated through these methods were incorporated as attribute data into GIS-based expressway features at a large scale and were subsequently aggregated and mapped as averages per route, corresponding to each row in the expressway attribute table.

#### 2.2 GIS-based data analysis method

Among the selected factors for large-scale analysis, hillshade, slope, and curvature were derived through spatial analysis; precipitation, humidity, and temperature were interpolated by the IDW method; and the density of 119 Emergency Rescue Centers was calculated via kernel density estimation. The hillshade factor (*H*) was derived using Eq. (1), based on a DEM with a spatial resolution of 5 m, representing elevation data across the entire territory of South Korea. The elevation values in the DEM range from -23.6896 to 2454.74 m. Higher elevations are associated with greater shadow intensity and steeper terrain features such as slope and curvature, thereby affecting the topographical characteristics of expressway segments.

The variables derived through DEM-based spatial analysis included hillshade, slope, and curvature. In Eq. (1),  $\theta_S$  denotes the solar elevation angle (in degrees),  $\varphi_S$  the solar azimuth angle,  $\theta_i$  the slope angle of the terrain (in degrees), and  $\varphi_i$  the terrain aspect angle. Solar elevation and azimuth data were obtained from the Astronomical Knowledge Information System of the Korea Astronomy and Space Science Institute. Jangyeon-ri, Cheongsung-myeon, Okcheon-gun, Chungcheongbuk-do was selected as the representative geographic center of South Korea for solar position reference. Average solar position values were computed for the time period from 08:00 to 13:00 during winter (December 2023 to February 2024). A raster-based average hillshade map was then generated from this data and incorporated as an input variable in the black ice vulnerability assessment.

$$H = 255 * \left(\cos \theta_s * \cos \theta_i + \sin \theta_s * \sin \theta_i * \cos(\varphi_s - \varphi_i)\right)$$
 (1)

Slope (S) was calculated using Eq. (2), derived from the DEM. In this equation,  $\partial Z/\partial x$  and  $\partial Z/\partial y$  represent the elevation gradients in the x- and y- directions of each grid cell, respectively. These gradients were computed using elevation differences between adjacent cells. The resulting slope values, initially calculated in radians, were converted to degrees by multiplying by a constant factor of  $180/\pi$ .<sup>(26)</sup>

$$S = \arctan\left(\sqrt{\left(\frac{\partial Z}{\partial x}\right)^2 + \left(\frac{\partial Z}{\partial y}\right)^2}\right) * \frac{180}{\pi}$$
 (2)

Curvature (C) was calculated using Eq. (3) based on a DEM. Curvature is a key topographic metric that describes how the terrain surface bends and how slope varies across space. Along with slope and aspect, it is widely used in terrain analysis to characterize surface form. In this context, curvature quantifies the rate of change in slope, indicating surface concavity or convexity. In Eq. (3),  $\frac{\partial^2 Z}{\partial x^2}$  and  $\frac{\partial^2 Z}{\partial y^2}$  represent the second-order partial derivatives of elevation in the x- and y- directions, respectively. These values were computed using elevation differences among neighboring grid cells in the DEM.<sup>(27)</sup>

$$C = \frac{\partial^2 Z}{\partial x^2} + \frac{\partial^2 Z}{\partial y^2} \tag{3}$$

Precipitation (P), humidity (Hu), and temperature (T) were estimated using Eq. (4) through IDW. Precipitation refers to the condensation of water vapor in either liquid or solid form that falls from the atmosphere to the ground, including phenomena such as rain, snow, sleet, hail, and blizzards. Owing to the spatial and seasonal variabilities of precipitation and temperature, particularly under climate change scenarios, these variables were included as key risk factors for roadway icing.<sup>(28)</sup>

Spatial interpolation was performed by the IDW method based on point observations of precipitation, humidity, and temperature. In this study, we applied this technique to estimate the value at a specific location by assigning weights to surrounding observations according to their distance. In Eq. (4), V(p) denotes the estimated value at location p,  $V_i$  is the observed value at neighboring point i,  $d(p, p_i)$  represents the distance between location p and point i, and p is the power parameter that controls the weighting function. Typically, the exponent p ranges from 1 to 3, with higher values assigning greater effect to nearer points. The interpolated raster maps of V(p) were clipped to the national expressway shapefile shown in Fig. 2(c), resulting in expressway-specific spatial layers for precipitation, humidity, and temperature. (29,30)

$$P,H,T=V(p) = \frac{\sum_{i=1}^{n} \left(\frac{v_i}{d(p,p_i)^p}\right)}{\sum_{i=1}^{n} \left(\frac{1}{d(p,p_i)^p}\right)}$$
(4)

The density of 119 Emergency Rescue Centers was calculated using Eq. (5) through kernel density estimation (KDE) based on point data. KDE is a spatial interpolation technique used to estimate and visualize the continuous distribution of point-based events over space. In Eq. (5), n is the total number of points, x is the location at which the density is estimated,  $x_i$  denotes the coordinates of point i, h is the bandwidth, d is the spatial dimensionality, and K is the kernel function. The bandwidth h determines the extent of smoothing; larger h values produce broader and smoother density surfaces. In this study, the spatial dimensionality d was set to 2, and a Gaussian kernel (i.e., normal distribution) was employed as the smoothing function. (31,32)

$$O = D(x) = \frac{1}{n * h^d} \sum_{i=1}^{n} K\left(\frac{x - x_i}{h}\right)$$
 (5)

#### 2.3 GIS-based vulnerability analysis method

For the GIS-based assessment of black ice traffic accident vulnerability, ten factors—hillshade, precipitation, humidity, temperature, slope, curvature, traffic volume, bridge length,

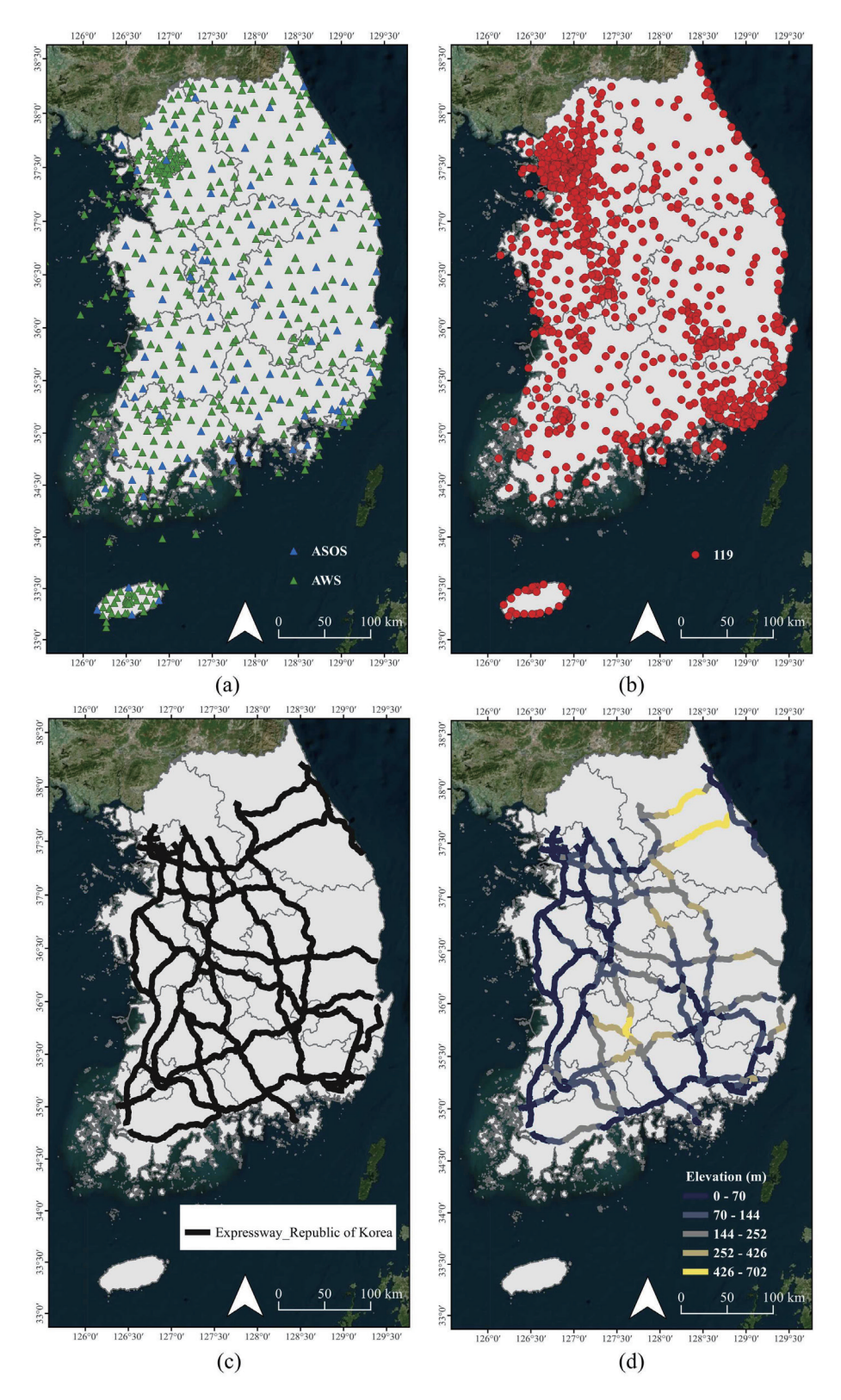


Fig. 2. (Color online) Construction of data layers for GIS-based vulnerability analysis: (a) locations of Automated Synoptic Observing Stations (ASOS) and Automated Weather Stations (AWS), (b) point data for 119 Emergency Rescue Centers used for kernel density estimation, (c) expressway attribute data including traffic volume, bridge length, and tunnel count, and (d) DEM overlaid on the national expressway network, used to derive hillshade, slope, and curvature. (Source: Bing Satellite provided via WMS, URL: <a href="https://ecn.t3.tiles.virtualearth.net/tiles/a{q}.jpeg?g=0&dir=dir\_n">https://ecn.t3.tiles.virtualearth.net/tiles/a{q}.jpeg?g=0&dir=dir\_n</a>, last accessed: 21 July 2024).

tunnel count, and 119 Emergency Rescue Center density—were classified into three categories, namely, exposure, sensitivity, and adaptive capacity, based on the IPCC Climate Change Vulnerability Assessment Framework. The classification scheme is shown in Table 1. Entropy-based weighting was then applied to determine the relative contribution of each factor to the overall vulnerability index.

Exposure refers to meteorological and environmental factors that contribute to the formation of black ice, including hillshade, precipitation, humidity, and temperature. Sensitivity refers to the physical and operational characteristics of expressways that interact with exposure conditions, such as slope, curvature, traffic volume, bridge length, and tunnel count. Adaptive capacity refers to the ability to mitigate accident-related impacts and is represented by the density of 119 Emergency Rescue Centers.

In this study, we aim to assess the large-scale vulnerability of black-ice-related traffic accidents across the national expressway network in South Korea using GIS. We also seek to provide foundational data for accident prevention planning and budget allocation by comprehensively incorporating multiple contributing factors. Entropy weighting was employed to evaluate the relative importance of each factor based on its variability. Concurrently, Euclidean distance was used to integrate the normalized variables and account for their combined effects. This approach allows for efficient integration within a GIS environment and facilitates the effective utilization of spatial information for vulnerability assessment.

Each factor was normalized using Eq. (6), where  $X_i$  represents the attribute value (i.e., expressway section) for variable j, and  $X_{min}$  and  $X_{max}$  are the minimum and maximum values of that variable, respectively. The normalized values range from 0 to 1. Entropy values  $(E_j)$  were then calculated using Eq. (7), where m is the total number of expressway sections and n is the number of variables. Greater variance among attribute values results in higher entropy. The constant k serves to adjust for the number of sections, ensuring that entropy values remain between 0 and 1. Diversity  $(d_j)$  was derived from the entropy values using Eq. (8), and final weights  $(w_j)$  were computed using Eq. (9). The results of this weighting process were then applied in subsequent steps of the methodology. This integrated approach enables objective weight assignment through entropy analysis while enhancing the spatial interpretability of risk by leveraging GIS visualization. As a result, the combination of these methods facilitates the prioritization of high-risk areas in a quantifiable and geographically meaningful manner.

$$N_i = \frac{X_i - X_{min}}{X_{max} - X_{min}} \tag{6}$$

$$E_{j} = -k \sum_{i=1}^{m} \ln p_{ij} \left( k = \frac{1}{\ln m}, j = 1, 2, ..., n \right)$$
 (7)

$$d_{i} = 1 - E_{i} \tag{8}$$

$$w_j = \frac{d_j}{\sum_{j=1}^n d_j} \tag{9}$$

Equation (10) presents the Euclidean distance formula used to calculate the overall vulnerability index by integrating the three components of the IPCC framework: exposure (E), sensitivity (S), and adaptive capacity (A).<sup>(34)</sup> All input variables were normalized to values ranging from 0 to 1 prior to their inclusion in the formula. Equation (11) defines the exposure index (E) as the weighted sum of four normalized factors: hillshade (H), precipitation (P), humidity (HU), and temperature (T). The associated entropy weights are denoted as  $w_H$ ,  $w_P$ ,  $w_{HU}$ , and  $w_T$ , respectively.

Equation (12) defines the sensitivity index (S) as the weighted sum of five normalized variables: slope (S), curvature (C), traffic volume (Tr), bridge length (B), and tunnel count (Tu). The corresponding entropy weights are denoted as  $w_S$ ,  $w_C$ ,  $w_{Tr}$ ,  $w_B$ , and  $w_{Tu}$ , respectively. Adaptive capacity (A) is represented by a single variable: the density of 119 Emergency Rescue Centers, which was already normalized and incorporated directly into Eq. (10).

$$V = \sqrt{E^2 + S^2 + (1 - A)^2} \tag{10}$$

$$E = w_H H + w_P P + w_{HU} H U + w_T T \tag{11}$$

$$S = w_S S + w_C C + w_{Tr} T r + w_R B + w_{Tu} T u$$
 (12)

#### 2.4 Study area and scenario selection

The national expressway network of South Korea was selected as the study area. Previous studies have shown that satellite-image-based spatial analysis, when combined with domestic topographic and meteorological data, offers sufficient precision for large-scale spatial modeling. Thirty major expressway routes with the highest traffic volumes were chosen, as listed in Table 2. The average annual traffic across these routes from 2018 to 2022 was 105,175 vehicles, indicating elevated vulnerability to traffic accidents due to substantial vehicle flow. Black ice poses a particularly serious threat on expressways during winter, as it forms suddenly and is difficult to detect visually, often resulting in fatal accidents. Topographic, meteorological, and traffic data were collected for the selected expressways. GIS layers were constructed using spatial analysis, point data interpolation, and kernel density estimation techniques. The resulting dataset was categorized into exposure, sensitivity, and adaptive capacity based on the IPCC Climate Change Vulnerability Assessment Framework, and the previously described GIS-based methodology was applied to integrate and analyze these variables.

Hillshade values range from 0 to 255, with higher values indicating greater surface illumination. The solar elevation and azimuth angles used for hillshade analysis were obtained

Busan Outer Ring Expressway

Seoul-Yangyang Expressway

Seoul Ring Expressway

Seocheon-Gongju Expressway

Seohaean Expressway

11

12

13

14

15

79155

162093

100035

138777

101004

|     | 1 2                             |                       | -   | ,                               |                       |
|-----|---------------------------------|-----------------------|-----|---------------------------------|-----------------------|
| No. | Expressway Name                 | Avg. Daily<br>Traffic | No. | Expressway Name                 | Avg. Daily<br>Traffic |
| 1   | Gyeongbu Expressway             | 497657                | 16  | Suncheon-Wanju Expressway       | 19163                 |
| 2   | Gyeongin Expressway             | 56788                 | 17  | Yeongdong Expressway            | 207226                |
| 3   | Gochang-Damyang Expressway      | 25756                 | 18  | Ulsan Expressway                | 29659                 |
| 4   | Gwangju-Daegu Expressway        | 32424                 | 19  | Iksan-Pohang Expressway         | 46616                 |
| 5   | Namhae Expressway               | 168913                | 20  | Second Gyeongin Expressway      | 29401                 |
| 6   | Namhae Branch Line 1            | 28816                 | 21  | Second Jungbu Expressway        | 126973                |
| 7   | Namhae Branch Line 2            | 47017                 | 22  | Jungbu Inland Expressway        | 89315                 |
| 8   | Dangjin-Yeongdeok Expressway    | 95342                 | 23  | Jungbu Inland Branch Expressway | 45966                 |
| 9   | Daejeon Southern Ring Road      | 24278                 | 24  | Jungbu Expressway               | 162093                |
| 10  | Donghae-Ulsan-Pohang Expressway | 72401                 | 25  | Jungang Expressway              | 185557                |

26

2.7

28

29

30

Jungang Branch Expressway

Tongyeong-Daejeon Expressway

Pyeongtaek-Jecheon Expressway

Honam Expressway

Honam Branch Expressway

57065

16733

332330

13914

162781

Table 2 Major expressways in South Korea and their average daily traffic volumes (2018–2022).

from the Astronomical Knowledge Information System. Hillshade, slope, and curvature were all derived from a DEM using Eqs. (1)–(3). Precipitation represents the total accumulation for the winter period of December 2023 to February 2024, while humidity and temperature denote averages for the same period. All meteorological data were obtained from the Weather Data Open Portal. The detailed scenario definitions and data sources for each variable used in the vulnerability analysis are shown in Table 3.

Traffic volume was derived from expressway section data spanning the years 2018 to 2022 and calculated as the average number of vehicles passing through each segment. Bridge length refers to the total span of bridges within each expressway section. Bridges are particularly susceptible to black ice formation owing to significant heat loss and shading effects caused by exposure on both the top and bottom surfaces, as well as at entry and exit points. Tunnel count indicates the number of tunnels in each section, with increased shading around tunnel entrances and exits also contributing to black ice risk. The data for bridges and tunnels were obtained from the National Spatial Information Platform and mapped onto the national expressway network. The density of 119 Emergency Rescue Centers was calculated using Eq. (5) and sourced from the Public Data Portal.

Figure 2(a) shows the locations of the Automated Synoptic Observing Stations (ASOS) and Automated Weather Stations (AWS) across South Korea<sup>(4)</sup>. The ASOS network consists of 97 stations, whereas the AWS network includes 515 stations. Weather data for winter 2023—specifically precipitation, humidity, and temperature—were obtained from these stations and interpolated by the IDW method. The point data were integrated into the GIS to generate continuous spatial layers for further analysis.

Figure 2(b) shows the point data for 119 Emergency Rescue Centers, which were processed using kernel density estimation to produce a continuous spatial distribution map. (36) Figure 2(c) includes traffic, bridge, and tunnel data layers derived from public transportation datasets. (38)

|                   |  |         |              |                     | •  |
|-------------------|--|---------|--------------|---------------------|--|
| Category          | Factor                                 | Unit    | Value range  | Data period         | Data source  |
|                   | Hillshade                              | _       | 63.64–116.96 | Dec. 2023–Feb. 2024 | DEM, Astronomical<br>Knowledge Information <sup>(37)</sup> |
| Evenogues         | Precipitation                          | mm      | 0-437.01     | Dec. 2023-Feb. 2024 | Weather Data Open Portal <sup>(4)</sup>                    |
| Exposure          | Humidity                               | %       | 0-80.26      | Dec. 2023-Feb. 2024 | Weather Data Open Portal <sup>(4)</sup>                    |
|                   | Temperature                            | °C      | -3.53-5.39   | Dec. 2023–Feb. 2024 | Weather Data Open Portal <sup>(4)</sup>                    |
|                   | Slope                                  | Degrees | 0-27.08      | _                   | DEM  |
|                   | Curvature                              | _       | -6.34-2.31   | _                   | DEM  |
| Sensitivity       | Traffic volume                         | Count   | 0-258,198    | Jan. 2018–Dec. 2022 | Expressway public data portal <sup>(38)</sup>              |
| Sensitivity       | Bridge length                          | m       | 0-8289.05    | _                   | National Spatial Information<br>Platform <sup>(39)</sup>   |
|                   | Tunnel count                           | Count   | 0-11         | _                   | National Spatial Information<br>Platform <sup>(39)</sup>   |
| Adaptive capacity | 119 Emergency Rescue<br>Center Density | _       | 0-0.05       | _                   | Public Data Portal <sup>(36)</sup>                         |

Table 3
Scenario definitions and data sources for factors used in black ice traffic accident vulnerability assessment.

These layers were spatially aligned with and clipped to the national expressway features illustrated in Fig. 2(d), which presents the DEM overlaid on the expressway network. Spatial analyses for hillshade, slope, and curvature were performed using this elevation dataset.<sup>(39)</sup>

#### 3. Results

The results are presented in three stages: data preprocessing, entropy-based weighting, and GIS-based vulnerability analysis. The dataset consists of ten variables classified according to the IPCC Climate Change Vulnerability Assessment Framework. Specifically, the exposure category includes hillshade, precipitation, humidity, and temperature; the sensitivity category includes slope, curvature, traffic volume, bridge length, and tunnel count; and the adaptive capacity category consists of the density of 119 Emergency Rescue Centers.

Hillshade, slope, and curvature were derived through spatial analysis, whereas precipitation, humidity, and temperature were interpolated by the IDW method. The density of 119 Emergency Rescue Centers was calculated using kernel density estimation. Entropy weighting was subsequently applied to determine the relative importance of each factor. A composite vulnerability index was then calculated by integrating exposure, sensitivity, and adaptive capacity. The final vulnerability results were visualized using GIS.

#### 3.1 Data preprocessing results

Figure 3 presents the raster-based preprocessing results for precipitation, humidity, temperature, and 119 Emergency Rescue Center density. Figures 3(a)–3(c) were generated by the IDW method, whereas Fig. 3(d) was produced by kernel density estimation.

Figure 3(a) shows the spatial distribution of precipitation, with a mean of 229.18 mm, a standard deviation of 79.62 mm, a maximum of 1028.24 mm, and a minimum of 18.07 mm.

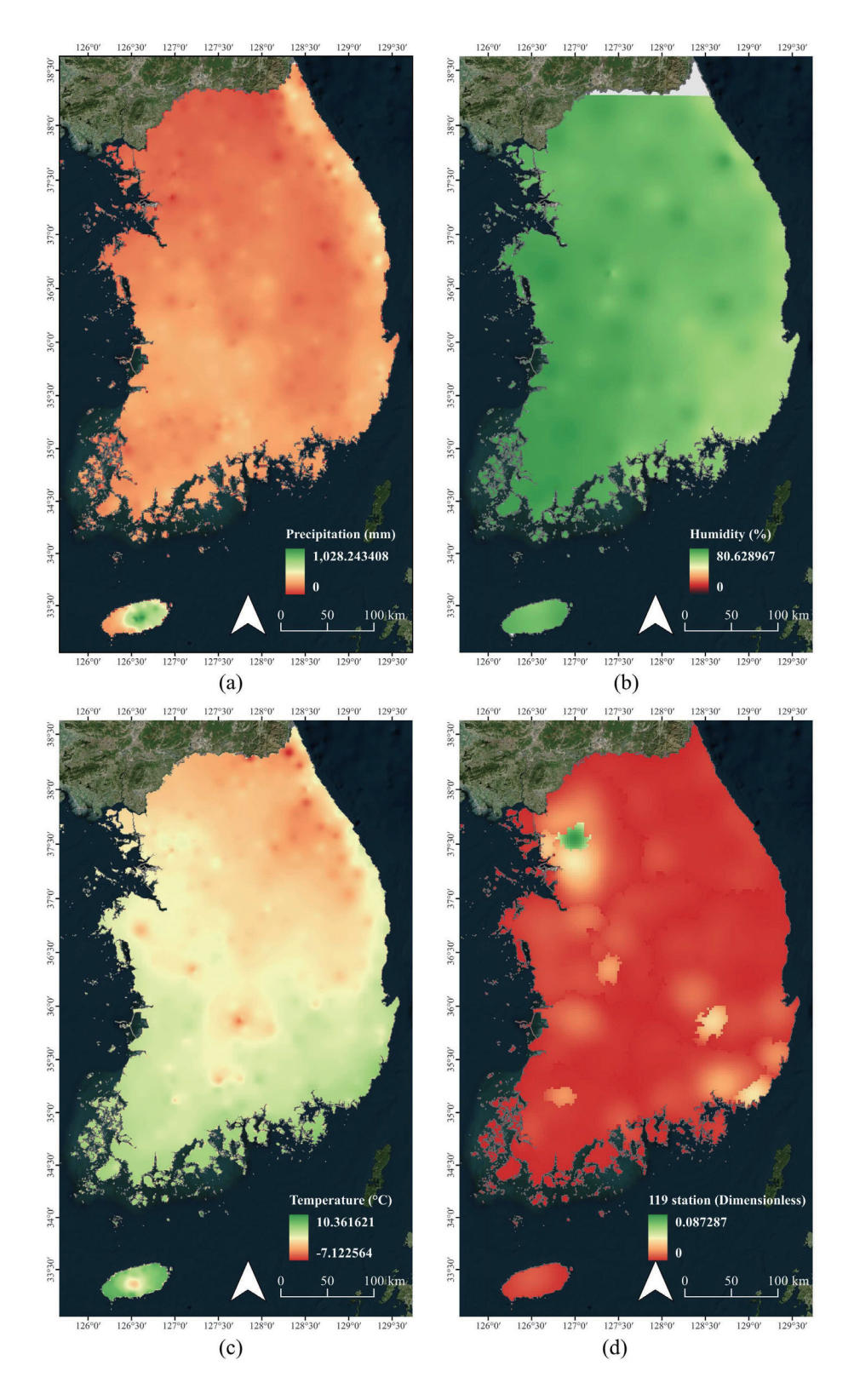


Fig. 3. (Color online) Preprocessing results of meteorological and spatial variables for GIS-based vulnerability analysis: (a) precipitation interpolated by inverse distance weighting (IDW), (b) humidity interpolated by IDW, (c) temperature interpolated by IDW, and (d) kernel density map of 119 Emergency Rescue Centers. (Source: Bing Satellite provided via WMS, URL: <a href="https://ecn.t3.tiles.virtualearth.net/tiles/a{q}.jpeg?g=0&dir=dir\_n">https://ecn.t3.tiles.virtualearth.net/tiles/a{q}.jpeg?g=0&dir=dir\_n</a>, last accessed: 21 July 2024).

Figure 3(b) shows the raster for humidity, with a mean of 80.63%, a standard deviation of 4.54%, a maximum of 80.65%, and a minimum of 57.69%. Figure 3(c) shows the temperature distribution, with a mean of 1.66 °C, a standard deviation of 2.24 °C, a maximum of 10.36 °C, and a minimum of -7.12 °C. Figure 3(d) presents the kernel density map of 119 Emergency Rescue Centers, with a mean value of 0.01, a standard deviation of 0.01, a maximum of 0.09, and a minimum of 0.

Figures 4 and 5 present GIS-based visualizations of the exposure variables. Figure 4 illustrates the preprocessing results of hillshade, which was obtained via spatial analysis and mapped onto the national expressway network. Figures 4(a)–4(f) show hillshade maps for each hour from 08:00 to 13:00, whereas Fig. 4(g) shows the average hillshade during that time period. For the 493 expressway sections, the average hillshade was 94.76, with a standard deviation of 6.40, a maximum of 116.96, and a minimum of 63.64 (unitless). Areas with lower hillshade values are more prone to shadows, and regions where shading persists across multiple time steps are considered more susceptible to black ice formation.

Figure 5 presents the exposure variables—precipitation, humidity, and temperature—after the interpolated raster layers from Fig. 3 were clipped to the national expressway features. Figure 5(a) shows the clipped precipitation layer, with a mean of 219.78 mm, a standard deviation of 56.56 mm, a maximum of 437.01 mm, and a minimum of 0 mm. Increased winter precipitation raises the likelihood of freezing rain, thereby increasing black ice risk. Figure 5(b) shows the humidity layer, with a mean of 70.97%, a standard deviation of 6.47%, a maximum of 80.26%,

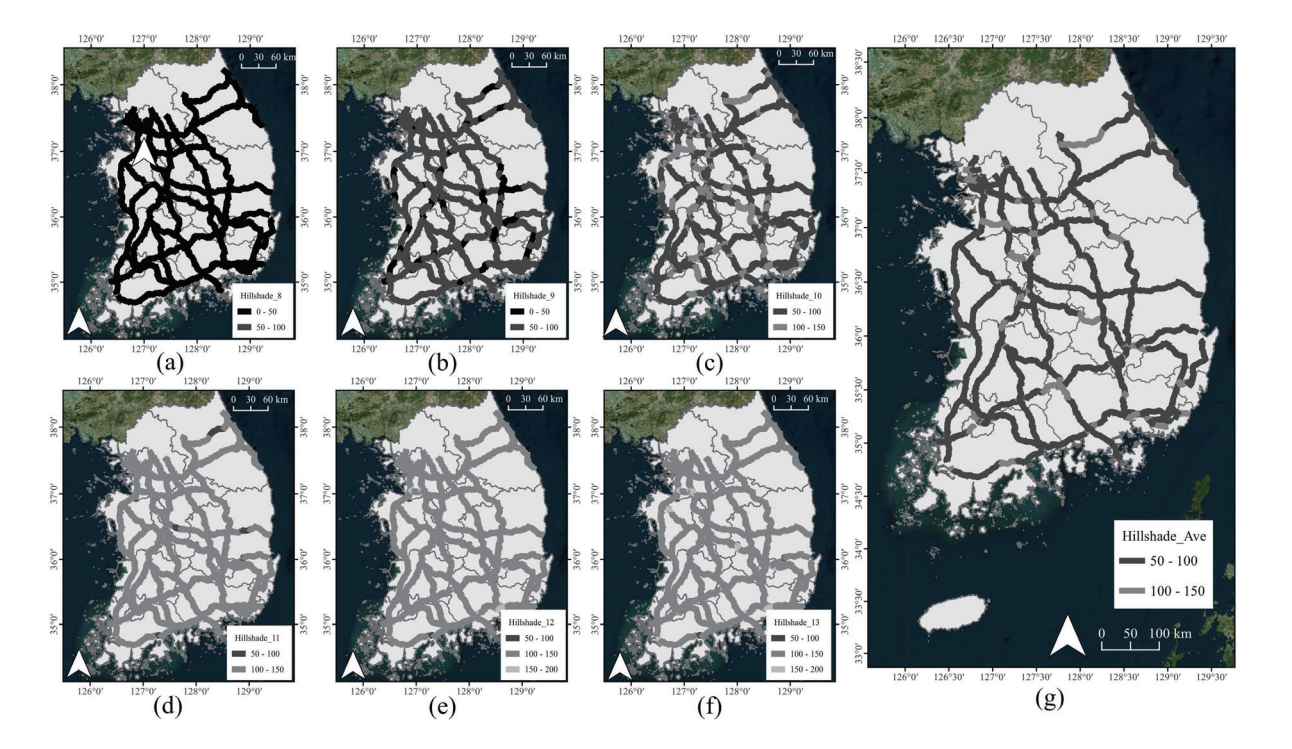


Fig. 4. (Color online) Spatial analysis results of hillshade between 08:00 and 13:00: (a)–(f) hourly hillshade maps at 1-h intervals from 08:00 to 13:00 and (g) average hillshade across all time intervals. (Source: Bing Satellite provided via WMS, URL: <a href="https://ecn.t3.tiles.virtualearth.net/tiles/a{q}.jpeg?g=0&dir=dir\_n">https://ecn.t3.tiles.virtualearth.net/tiles/a{q}.jpeg?g=0&dir=dir\_n</a>, last accessed: 21 July 2024).

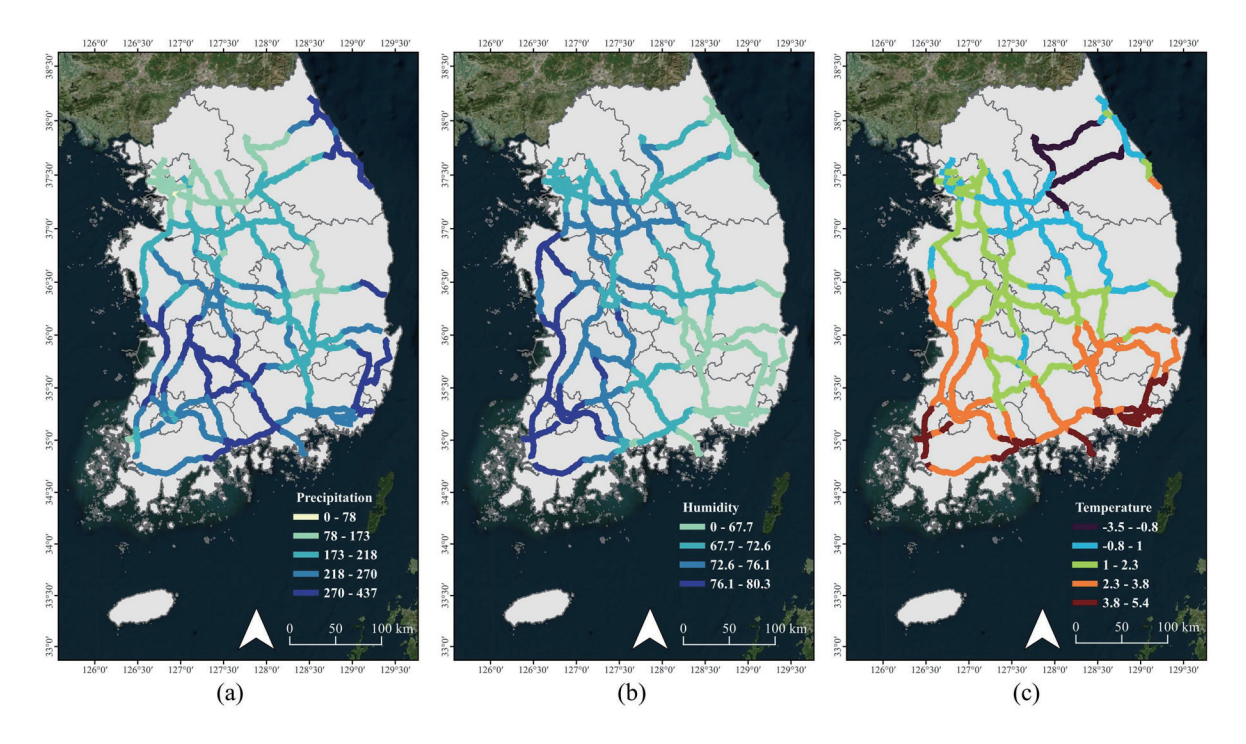


Fig. 5. (Color online) GIS visualization of exposure variables: (a) precipitation interpolated and clipped to the national expressway network, (b) humidity interpolated and clipped to the national expressway network, and (c) temperature interpolated and clipped to the national expressway network. (Source: Bing Satellite provided via WMS, URL: <a href="https://ecn.t3.tiles.virtualearth.net/tiles/a{q}.jpeg?g=0&dir=dir\_n">https://ecn.t3.tiles.virtualearth.net/tiles/a{q}.jpeg?g=0&dir=dir\_n</a>, last accessed: 21 July 2024).

and a minimum of 0%. Higher humidity levels promote frost accumulation, further contributing to black ice formation. Figure 5(c) shows the temperature distribution, with a mean of 2.01 °C, a standard deviation of 1.58 °C, a maximum of 5.39 °C, and a minimum of -3.53 °C. Lower average temperatures in expressway segments are associated with an increased probability of subfreezing conditions and thus a higher black ice risk.

Figure 6 shows the GIS-based visualizations of the sensitivity and adaptive capacity variables. Figures 6(a)–6(e) depict the five sensitivity factors, whereas Fig. 6(f) shows the adaptive capacity layer. Figure 6(a) shows the slope of expressway sections, derived from spatial analysis, with a mean of 7.5°, a standard deviation of 4.86°, a maximum of 27.08°, and a minimum of 0°. Steeper slopes reduce tire–road friction under black ice conditions, increasing the risk of accidents. Figure 6(b) illustrates road curvature, also obtained through spatial analysis, with a mean of 0.15, a standard deviation of 0.52, a maximum of 2.31, and a minimum of -6.34. Greater curvature increases the difficulty of vehicle control on slippery road surfaces. Figure 6(c) presents the average daily traffic volume, with a mean of 62073 vehicles, a standard deviation of 51342.77, a maximum of 258198, and a minimum of 0. Sections with higher traffic volumes are more exposed to accident risk under black ice conditions due to greater vehicle density. Figure 6(d) shows the total bridge length per section, with a mean of 1,452.06 m, a standard deviation of 1,219.44 m, a maximum of 8289.05 m, and a minimum of 17.05 m. Bridges are highly susceptible to heat loss and freezing due to exposure on both surfaces, increasing

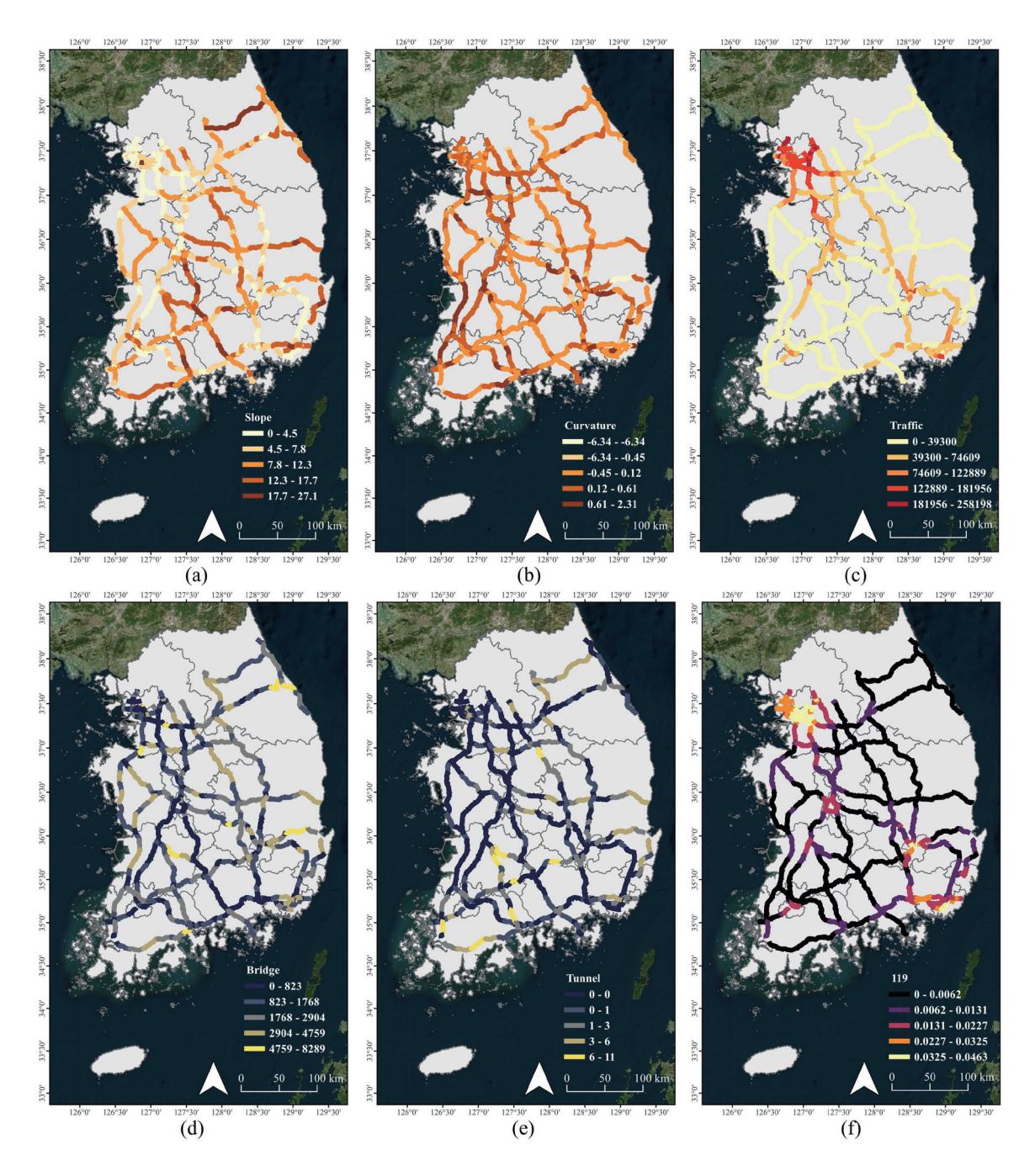


Fig. 6. (Color online) GIS visualizations of sensitivity and adaptive capacity variables: (a) slope (degrees), (b) curvature (unitless), (c) traffic volume (vehicles/day), (d) total bridge length (m), (e) number of tunnels, and (f) density of 119 Emergency Rescue Centers. (Source: Bing Satellite provided via WMS, URL: <a href="https://ecn.t3.tiles.virtualearth.net/tiles/a{q}.jpeg?g=0&dir=dir\_n">https://ecn.t3.tiles.virtualearth.net/tiles/a{q}.jpeg?g=0&dir=dir\_n</a>, last accessed: 21 July 2024).

black ice risk. Figure 6(e) depicts the number of tunnels per expressway section, with a mean of 2.33, a standard deviation of 1.93, a maximum of 11, and a minimum of 1. Tunnel entrances and exits are typically shaded and cooler, elevating the likelihood of black ice formation. Figure 6(f)

shows the clipped density of 119 Emergency Rescue Centers, derived from Fig. 3(d). The mean density is 0.01, with a standard deviation of 0.01, a maximum of 0.05, and a minimum of 0. Higher rescue center density improves emergency response capabilities and enhances adaptive capacity in the event of black-ice-related accidents.

#### 3.2 Entropy analysis results

Table 4 shows the vulnerability factors along with their corresponding entropy weights. Entropy-based weighting was applied to the exposure and sensitivity categories, each consisting of multiple variables. In contrast, the adaptive capacity category, which contains only a single factor—119 Emergency Rescue Center density—was assigned a fixed weight of 1.

In the exposure category, humidity had the highest weight (0.36), followed by precipitation (0.26), temperature (0.20), and hillshade (0.18). In the sensitivity category, slope received the highest weight (0.25), followed by traffic volume (0.23), tunnel count (0.22), bridge length (0.19), and curvature (0.10).

These entropy-based weights were subsequently applied to the normalized values of each factor to compute the composite vulnerability index for all expressway segments. On the basis of this index, a series of spatial analyses was conducted using GIS to generate vulnerability maps that highlight high-risk areas. The following section presents the results of this spatial mapping.

#### 3.3 Black ice traffic accident vulnerability map results

Figure 7 shows GIS-based mapping results of black ice traffic accident vulnerability, calculated using entropy-weighted exposure, sensitivity, and adaptive capacity indices. Figure 7(a) shows the exposure index computed using Eq. (11), with a mean of 0.50, a standard deviation of 0.09, a maximum of 0.77, and a minimum of 0.33. Figure 7(b) illustrates the sensitivity index calculated via Eq. (12), with a mean of 0.25, a standard deviation of 0.08, a maximum of 0.56, and a minimum of 0.10. Figure 7(c) presents the final vulnerability map derived from Eq. (10), with a mean of 0.96, a standard deviation of 0.20, a maximum of 1.29, and a minimum of 0.48. All indices are unitless and normalized between 0 and 1, enabling direct spatial comparison.

Table 4
Entropy weights assigned to vulnerability assessment factors.

| Vulnerability category | Factor                      | Weight |
|------------------------|-----------------------------|--------|
|                        | Hillshade                   | 0.18   |
| Evenogues              | Precipitation               | 0.26   |
| Exposure               | Humidity                    | 0.36   |
|                        | Temperature                 | 0.2    |
|                        | Slope                       | 0.25   |
|                        | Curvature                   | 0.1    |
| Sensitivity            | Traffic volume              | 0.23   |
|                        | Bridge length               | 0.19   |
|                        | Tunnel count                | 0.22   |
| Adaptive capacity      | 119 Emergency Rescue Center | 1      |

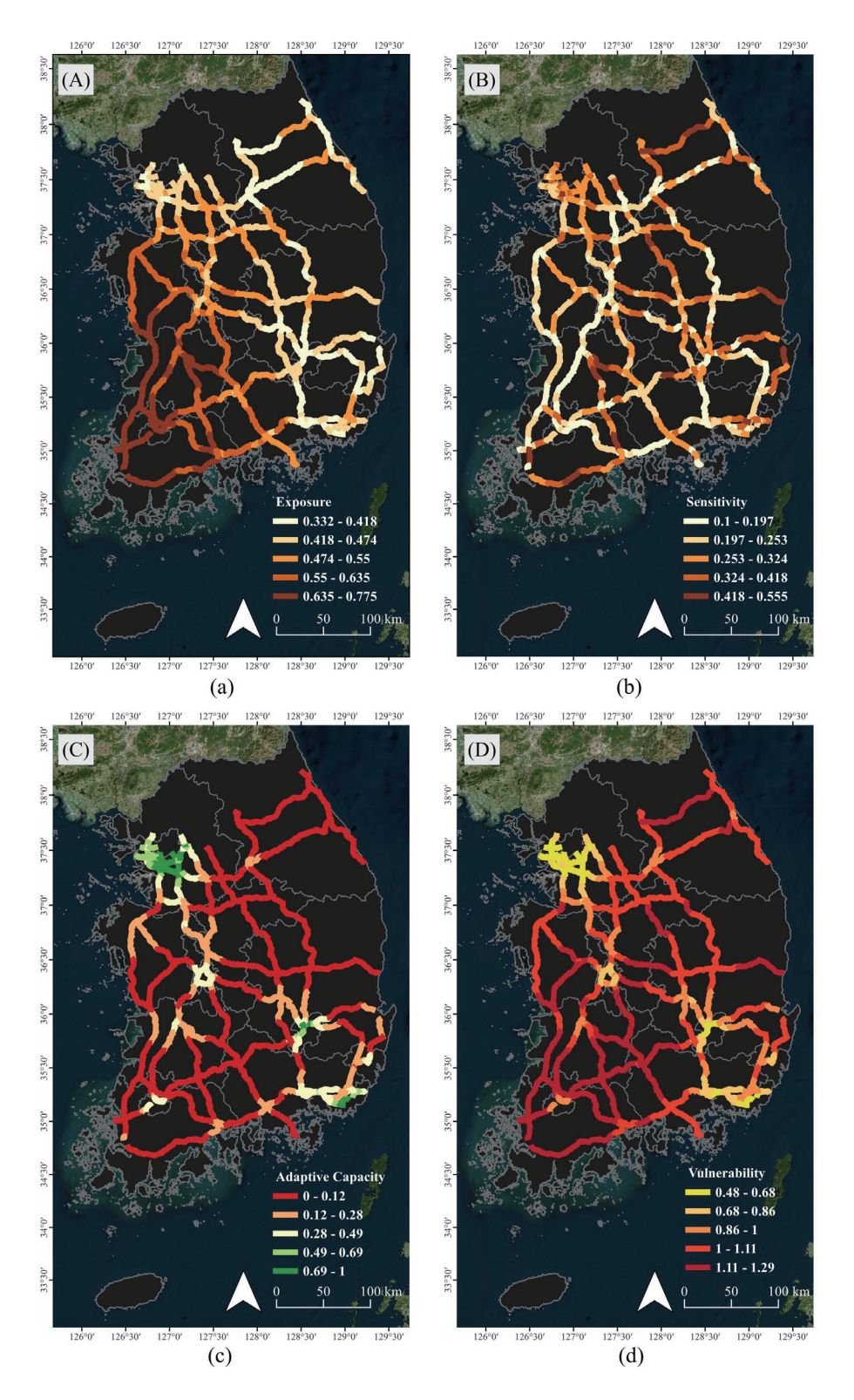


Fig. 7. (Color online) GIS-based vulnerability assessment results: (a) exposure index, calculated from hillshade, precipitation, humidity, and temperature, (b) sensitivity index, based on slope, curvature, traffic volume, bridge length, and tunnel count, (c) adaptive capacity, represented by the normalized density of 119 Emergency Rescue Centers, and (d) composite vulnerability index for black-ice-related traffic accidents, classified into five grades using the Natural Breaks method (Grade 1: 0.48–0.69; Grade 2: 0.70–0.86; Grade 3: 0.86–1.00; Grade 4: 1.00–1.11; Grade 5: 1.11–1.29). (Source: Bing Satellite provided via WMS, URL: <a href="https://ecn.t3.tiles.virtualearth.net/tiles/a{q}.jpeg?g=0&dir=dir\_n">https://ecn.t3.tiles.virtualearth.net/tiles/a{q}.jpeg?g=0&dir=dir\_n</a>, last accessed: 21 July 2024).

Adaptive capacity, based on the normalized density of 119 Emergency Rescue Centers, exhibited a mean of 0.24, a standard deviation of 0.23, a maximum of 1.00, and a minimum of 0. The final vulnerability index was classified into five grades using the Natural Breaks method, which identifies inherent groupings within the data by maximizing interclass variance. The resulting classification thresholds were as follows.

- Grade 1: 0.48-0.69
- Grade 2: 0.70-0.86
- Grade 3: 0.86-1.00
- Grade 4: 1.00-1.11
- Grade 5: 1.11-1.29

This classification scheme effectively reveals spatial patterns and allows for a clear differentiation of regions with elevated vulnerability to black-ice-related traffic accidents.

#### 4. Discussion

#### 4.1 Black ice traffic accident vulnerability map analysis

We conducted a large-scale vulnerability assessment of black-ice-related traffic accidents across South Korea's national expressway network. Ten variables were categorized according to the IPCC vulnerability framework and integrated using GIS-based spatial analysis with entropy weighting to produce a composite vulnerability index for each expressway section. The resulting index ranged from 0.48 to 1.29, with a mean of 0.96 and a standard deviation of 0.20. The index values were classified into five grades using the Natural Breaks method. Sections with values exceeding 1.11 were classified as Grade 5, representing the highest level of vulnerability. These high-risk segments are typically associated with a combination of adverse topographic, meteorological, and infrastructural conditions, along with limited access to emergency response services. Therefore, they should be prioritized for intervention measures and resource allocation within black ice accident prevention strategies.

Among the exposure factors, humidity (mean: 70.97%, weight: 0.36) emerged as the most influential variable, suggesting that condensation and frost accumulation may contribute more significantly to black ice formation than temperature alone. Precipitation (219.78 mm), temperature (2.01 °C), and hillshade (94.76) also played substantial roles in promoting surface icing conditions. Within the sensitivity category, slope (mean: 7.5°, maximum: 27.08°, weight: 0.25) and traffic volume (mean: 62,072 vehicles, maximum: 258,198 vehicles, weight: 0.23) were identified as the dominant contributors. Curvature, bridge length, and tunnel count further increased structural and operational complexity, exacerbating vulnerability. Adaptive capacity, represented by the density of 119 Emergency Rescue Centers, exhibited a low mean of 0.01 and a maximum of 0.05, indicating limited emergency response infrastructure across certain expressway sections. Sections classified as Grade 5 exhibited overlapping vulnerabilities across meteorological, structural, traffic, and response dimensions. These segments are not only more prone to black ice accidents but also more susceptible to severe damage propagation. The findings underscore the necessity of adopting multidimensional risk assessment frameworks that incorporate interactions among diverse contributing factors, rather than relying solely on isolated indicators.

In this study, we developed a black ice traffic accident vulnerability map to provide actionable reference data for expressway management agencies to prioritize interventions by season and region. In high-risk areas (Grade 5), the targeted deployment of innovative safety signage, high-friction pavement materials, and automated snow removal systems is recommended. Conversely, in low-vulnerability sections, resource allocation may be directed toward preventive monitoring and early warning strategies. In addition to operational deployment, the map demonstrates high applicability for policy integration—supporting proactive budget allocation, winter safety inspection planning, and the incorporation of black ice accident prediction models. Ultimately, a robust quantitative foundation for risk-based resource management is established, and a basis for the development of real-time, weather-traffic-integrated alert systems and simulation-driven preemptive response frameworks is provided.

### 4.2 Black ice traffic accident vulnerability spatial autocorrelation analysis

To evaluate the spatial validity of the vulnerability index, a spatial autocorrelation analysis was conducted in accordance with Tobler's First Law of Geography: "everything is related to everything else, but near things are more related than distant things". (40) Moran's Index (Moran's *I*) was employed to quantify the degree of spatial clustering observed in the vulnerability map presented in Fig. 7.

Moran's I ranges from -1 to +1.

- Values close to +1 indicate strong positive spatial autocorrelation (i.e., clustering of similar values),
- Values near –1 indicate negative spatial autocorrelation (i.e., clustering of dissimilar values), and
- Values around 0 suggest spatial randomness.

The computation follows the formulation defined in Eq. (13), where the parameters are as follows.

- N: total number of spatial units (observations)
- X: attribute value of each spatial unit
- $\overline{X}$ : mean of all attribute values
- $w_{ii}$ : spatial weight between units i and j
- W: sum of all spatial weights

In this study, the spatial weights were defined using the inverse distance method based on Euclidean distance.

Table 5 shows the results of the spatial autocorrelation analysis for the vulnerability index. Moran's I was calculated as 0.625650, with an expected E(I) of -0.002033, a variance of 0.000126, a Z-score of 55.87, and a p-value of less than 0.000001. At a significance level of  $\alpha = 0.05$ , the p-value indicates that the observed Moran's I is statistically significant, allowing the rejection of the null hypothesis of spatial randomness. This result suggests that the vulnerability index exhibits strong positive spatial autocorrelation, thereby supporting the spatial coherence and structural validity of the GIS-based vulnerability model.

Table 5
Results of spatial autocorrelation analysis for black ice traffic accident vulnerability (Moran's I method).

| Metric                | Value      |  |  |
|-----------------------|------------|--|--|
| Moran's Index (I)     | 0.625650   |  |  |
| Expected Index $E(I)$ | -0.002033  |  |  |
| Variance              | 0.000126   |  |  |
| z-score               | 55.869821  |  |  |
| <i>p</i> -value       | < 0.000001 |  |  |

Moran's Index(I) = 
$$\frac{W}{N} \frac{\sum_{i=1}^{N} \sum_{j=1}^{N} w_{ij} (X_i - \overline{X}) (X_j - \overline{X})}{\sum_{i=1}^{N} (X_i - \overline{X})^2}$$
(13)

In this validation step, the null hypothesis  $(H_0)$  assumes spatial randomness in the simulation results, whereas the alternative hypothesis  $(H_1)$  posits the existence of spatial clustering or regularity. The statistical significance of spatial autocorrelation is assessed on the basis of the p-value derived from the Z-score associated with Moran's I.

If the p-value is less than or equal to 0.05 (i.e., at the 5% significance level), the null hypothesis ( $H_0$ ) is rejected in favor of the alternative hypothesis ( $H_1$ ), indicating that the spatial pattern is statistically significant. The p-value is derived from the standard normal distribution using the Z-score, which quantifies the deviation of the observed Moran's I from its expected value under the null hypothesis. The calculated Z-score lies in the extreme right tail of the normal distribution, indicating strong positive spatial autocorrelation.

The Z-score is calculated using Eq. (14), where I is the observed Moran's Index, E[I] is its expected value under spatial randomness, and Variance refers to the variance of I across all spatial units.

$$Z\text{-}score = \frac{I - E[I]}{\sqrt{Variance}}$$
 (14)

The resulting p-value approached zero, providing compelling evidence to reject the null hypothesis ( $H_0$ ) in favor of the alternative hypothesis ( $H_1$ ). Accordingly, the black ice traffic accident vulnerability map exhibits statistically significant positive spatial autocorrelation, thereby validating the spatial integrity of the GIS-based simulation.

Hypothesis Test:

- $H_0$ : The black ice traffic accident vulnerability map exhibits no spatial autocorrelation. (Rejected)
- $H_1$ : The black ice traffic accident vulnerability map exhibits spatial autocorrelation. (Accepted)

#### 5. Conclusions

In this study, we conducted a nationwide case analysis of South Korea's expressway network to evaluate the vulnerability of black-ice-related traffic accidents on a large spatial scale. Ten contributing factors were selected on the basis of the IPCC Climate Change Vulnerability Assessment Framework, normalized using GIS, and integrated into a spatial vulnerability index through an entropy-weighted Euclidean distance approach. This methodology enabled a comprehensive quantitative assessment that incorporated topographic, meteorological, traffic, and emergency response characteristics across expressway sections.

The vulnerability index ranged from 0.48 to 1.29, with a mean of 0.96 and a standard deviation of 0.20. These values were classified into five vulnerability grades using the Natural Breaks method. Among the input variables, humidity (mean: 70.97%, weight: 0.36), slope (mean: 7.5°, weight: 0.25), and traffic volume (mean: 62073 vehicles, weight: 0.23) received the highest entropy weights, underscoring their substantial effect on accident vulnerability. A higher entropy weight reflects a greater spatial variability in a given factor, thereby increasing its relative contribution to the composite vulnerability index.

The resulting vulnerability map serves not only as a visual representation of weather-related risk but also as a policy-relevant decision-support tool that spatially integrates multiple complex factors. Spatial autocorrelation analysis validated the structural reliability of the model, yielding a Moran's I of 0.63 with a p-value < 0.000001, indicating statistically significant clustering in vulnerability patterns. These findings provide a practical foundation for expressway management agencies to identify and prioritize high-risk segments by season and region, thereby enabling a more efficient allocation of safety resources and infrastructure investment.

In particular, high-risk areas (Grade 5) should be prioritized for the deployment of advanced warning systems, high-friction pavement treatments, and automated snow and ice removal equipment. The vulnerability map developed in this study holds potential for further advancement into a real-time operational platform through integration with weather—traffic data fusion systems and AI-based accident prediction models.

However, in this study, we acknowledge limitations arising from the temporal scope of the weather data (limited to winter 2023–2024) and from the resolution and completeness of certain traffic and infrastructure datasets. Future research would benefit from the incorporation of multi-year climatic averages, real-time traffic flow information, and high-resolution terrain models to improve the accuracy, robustness, and practical applicability of the vulnerability assessment.

Despite these limitations, we addressed the shortcomings of previous studies—namely, their regional scope and reliance on single-factor analyses—by introducing a comprehensive, GIS-based vulnerability assessment model at the national expressway scale. The framework presented herein provides a robust foundation for future risk-based transportation safety planning and spatial decision-support systems.

## Acknowledgments

This study was supported by a grant from the National Research Foundation, Korea (NRF), funded by the Korean government (MSIT) (No. 2021R1C1C2010999).

This research was carried out while Seok Bum Hong was a Ph.D. student and later a postdoctoral researcher at Sungkyunkwan University. At the time of submission, he was no longer affiliated with the university and had joined the Korea Railroad Research Institute.

#### References

- 1 L. Cary: Black Ice (Vintage, New York, 2010).
- 2 C. Hull: Poetry Rev. 89 (1999) 23.
- 3 K. H. Kim: <a href="https://www.yna.co.kr/view/AKR20210210121400530">https://www.yna.co.kr/view/AKR20210210121400530</a> (accessed January 20, 2024).
- 4 Korea Meteorological Administration: Weather Data Open Portal: <a href="https://data.kma.go.kr/cmmn/main.do">https://data.kma.go.kr/cmmn/main.do</a> (accessed March 17, 2024).
- 5 E. G. Lee: https://www.asiae.co.kr/article/2019121419465391563 (accessed January 20, 2024).
- 6 S. E. Shin: https://www.seoul.co.kr/news/society/2020/01/06/20200106800006 (accessed January 19, 2024).
- 7 S. B. Hong, H. S. Yun, S. G. Yum, S. Y. Ryu, I. S. Jeong, and J. Kim: Nat. Hazards Earth Syst. Sci. **22** (2022) 3435. https://doi.org/10.5194/nhess-22-3435-2022
- 8 S.-B. Hong, B.-W. Lee, C.-H. Kim, and H.-S. Yun: Appl. Sci. 11 (2021) 8537. <a href="https://doi.org/10.3390/appl1188537">https://doi.org/10.3390/appl1188537</a>
- 9 Ş. Bilaşco and T.-C. Man: Appl. Sci. 14 (2024) 2643. https://doi.org/10.3390/app14062643
- 10 M. Eltemasi and H. Behtooiey: Heliyon 10 (2024) e28536. https://doi.org/10.1016/j.heliyon.2024.e28536
- 11 H.-C. Yang, M.-Q. Chen, and I.-L. Lin: Sens. Mater. 36 (2024) 1243. https://doi.org/10.18494/SAM4868
- 12 M.-S. Park, M. Kang, S.-H. Kim, H.-C. Jung, S.-B. Jang, D.-G. You, and S.-H. Ryu: Atmosphere **31** (2021) 525. https://doi.org/10.14191/Atmos.2021.31.5.525
- 13 T. DiLorenzo and X. Yu: Accid. Anal. Prev. 191 (2023) 107197. https://doi.org/10.1016/j.aap.2023.107197
- 14 T. Liu, Q. Pan, J. Sanchez, S. Sun, N. Wang, and H. Yu: IEEE Intell. Transp. Syst. Mag. **9** (2017) 91. <a href="https://doi.org/10.1109/MITS.2017.2666587">https://doi.org/10.1109/MITS.2017.2666587</a>
- 15 R. Xie, C. Liao, X. Luo, H. Guo, Z. Huang, and W. Peng: Front. Earth Sci. 11 (2023) 1251635. <a href="https://doi.org/10.3389/feart.2023.1251635">https://doi.org/10.3389/feart.2023.1251635</a>
- 16 H.-G. Kwon, H. Yang, and C. Yi: Remote Sens. 14 (2022) 6379. https://doi.org/10.3390/rs14246379
- B. Liu, S. Yan, H. You, Y. Dong, Y. Li, J. Lang, and R. Gu: Comput. Ind. 99 (2018) 294. <a href="https://doi.org/10.1016/j.compind.2018.03.026">https://doi.org/10.1016/j.compind.2018.03.026</a>
- 18 T. Nowrin and T. J. Kwon: Cold Reg. Sci. Technol. 202 (2022) 103631. <a href="https://doi.org/10.1016/j.coldregions.2022.103631">https://doi.org/10.1016/j.coldregions.2022.103631</a>
- 19 T. Eom, Y. Kwon, and H. Ko: Sens. Mater. 33 (2021) 2763. https://doi.org/10.18494/SAM.2021.3361
- 20 J. H. Lee and S. K. Choi: Crisisonomy 16 (2020) 109. https://doi.org/10.14251/crisisonomy.2020.16.2.109
- 21 J. Jang: Transp. Res. Interdiscip. Perspect. **29** (2025) 101299. <a href="https://doi.org/10.1016/j.trip.2024.101299">https://doi.org/10.1016/j.trip.2024.101299</a>
- 22 J. Kim, E. Kim, and D. Kim: Remote Sens. 14 (2022) 5252. https://doi.org/10.3390/rs14205252
- 23 A. Aggarwal, N. Bhattacharjee, A. Bhattacharya, R. Bose, A. Gupta, D. Gupta, A. Kapoor, and E. Rani: arXiv preprint arXiv:2010.12983 (2020). https://doi.org/10.48550/arXiv.2010.12983
- 24 S. Roy, R. G. De Anna, M. Mehregani, and E. Zakar: Sens. Mater. 12 (2000) 1.
- 25 J. Sharma and N. H. Ravindranath: Environ. Res. Commun. 1 (2019) 051004. https://doi.org/10.1088/2515-7620/
- 26 Raster Terrain Analysis QGIS Documentation: <a href="https://docs.qgis.org/3.40/en/docs/user\_manual/processing\_algs/qgis/rasterterrainanalysis.html">https://docs.qgis.org/3.40/en/docs/user\_manual/processing\_algs/qgis/rasterterrainanalysis.html</a> (accessed February 16, 2024).
- 27 R.Param.Scale GRASS GIS manual: <a href="https://grass.osgeo.org/grass-stable/manuals/r.param.scale.html">https://grass.osgeo.org/grass-stable/manuals/r.param.scale.html</a> (accessed February 16, 2024).
- 28 Z. Chu, L. Wang, Y. Ji, B. Zhou, J. Gong, Q. Wang, and L. Chen: Sens. Mater. **37** (2025) 1491. <a href="https://doi.org/10.18494/SAM5386"><u>https://doi.org/10.18494/SAM5386</u></a>
- 29 D. Shepard: Proc. 23rd ACM National Conf. (ACM, 1968) 517-524. https://doi.org/10.1145/800186.810616
- 30 K. Jaemyeong, C. Yunsoo, Y. Hasu, and L. Wonjong: Sens. Mater. 31 (2019) 2607. <a href="https://doi.org/10.18494/SAM.2019.2607">https://doi.org/10.18494/SAM.2019.2607</a>

- 31 A. Okabe, T. Satoh, and K. Sugihara: Int. J. Geogr. Inf. Sci. 23 (2009) 7. https://doi.org/10.1080/13658810802475491
- 32 Q.-J. Wang, Z.-H. Wang, J.-L. Zhou, and S. Dong: Sens. Mater. **32** (2020) 2942. <a href="https://doi.org/10.18494/SAM.2020.2942">https://doi.org/10.18494/SAM.2020.2942</a>
- 33 S. Duan, L. Zhang, and W.-L. Hsu: Sens. Mater. 32 (2020) 2719. https://doi.org/10.18494/SAM.2020.2719
- 34 J. G. Langdon and J. J. Lawler: Ecosphere 6 (2015) 1. https://doi.org/10.1890/ES14-00400.1
- 35 T. D. Acharya, I. T. Yang, and D. H. Lee: Sens. Mater. 30 (2018) 1866. https://doi.org/10.18494/SAM.2018.1866
- 36 P. D. Portal: Status of 119 Safety Centers and Other Sources <a href="https://www.data.go.kr/data/15065056/fileData.do">https://www.data.go.kr/data/15065056/fileData.do</a> (accessed February 17, 2024).
- 37 Korea Astronomy and Space Science Institute: Astronomical Knowledge Information: Solar Altitude and Azimuth Calculator, <a href="https://astro.kasi.re.kr/life/pageView/10">https://astro.kasi.re.kr/life/pageView/10</a> (accessed March 17, 2024).
- 38 Korea Expressway Corporation: Highway Public Data Portal <a href="https://data.ex.co.kr/">https://data.ex.co.kr/</a> (accessed February 19, 2024).
- 39 National Geographic Information Institute: National Spatial Data Platform, <a href="https://map.ngii.go.kr/mn/mainPage.do">https://map.ngii.go.kr/mn/mainPage.do</a> (accessed February 16, 2024).
- 40 H. J. Miller: Ann. Assoc. Am. Geogr. 94 (2004) 284. https://doi.org/10.1111/j.1467-8306.2004.09402005.x